Coordination chemistry of manganese and iron with N,O-donor ligands: oxidation catalysis and magnetochemistry of clusters

Godbole, M.D.

5

High-Nuclearity Manganese and Iron Complexes with the Anionic Ligand Methyl Salicylimidate*

*The three novel clusters $[Mn_6O_4(OMe)_2(OAc)_4(Mesalim)_4]$ (**3**), $[Mn_8O_2(OH)_2(OMe)_{12}(OAc)_2(Mesalim)_4]$ (**4**) and $[Fe_{10}O_4(OMe)_{14}Cl_2(Mesalim)_6]$ (**5**) have been synthesized from a simple didentate ligand HMesalim (HMesalim = methyl salicylimidate). Starting from the mononuclear complex $[Mn(Mesalim)_2(OAc)(MeOH)]$•MeOH (**1**), either the hexanuclear complex **3** or the octanuclear complex **4** is obtained after recrystallization, depending upon the reaction conditions and solvents used. Similarly, starting from the purple-colored mononuclear complex $[Fe(Mesalim)_2Cl]$ (**2**) the orange-colored decanuclear iron(III) cluster **5** has been obtained upon recrystallization from methanol. Complex **3** has a face-sharing double-cubane $[Mn_6O_6]$ core, unique in transition metal chemistry. Compounds **4** and **5** are composed of $[M_3O_4]$ partial cubanes. All complexes belong to a class of oxo-bridged cubic close-packed (ccp) molecular clusters resembling the metal oxide/hydroxide ores. Complex **4** exhibits intramolecular ferromagnetic interactions as evidenced from DC magnetic susceptibility studies (1.8 K – 300 K), resulting in a high-spin ground state, probably with $S_T = 8$. Complex **4** displays single molecule magnet (SMM) behavior as indicated by frequency and temperature dependences of its AC susceptibility. An Arrhenius plot gave relatively large experimental activation energy of 36.0 K. The magnetic properties of complexes **3** and **5** are dominated by antiferromagnetic interactions leading to zero-spin ground states.*

* This chapter is based on: Godbole, M. D.; Roubeau, O.; Clerac, R.; Kooijman, H.; Spek, A. L.; Bouwman, E., *Chem. Commun.* 2005, 3715-3717; Godbole, M. D.; Roubeau, O.; Clerac, R.; Kooijman, H.; Mills, A. M.; Spek, A. L.; Bouwman, E., *manuscript in preparation.*

5.1 Introduction

The design and synthesis of novel polynuclear manganese and iron clusters with primarily oxygen and nitrogen coordination are active areas of current chemical research. Clusters comprising manganese or iron ions are present in several metalloenzymes and metalloproteins ranging from the protein ferritin,[1, 2] responsible for iron storage, to the water oxidizing complex of photosystem II of bacterial photosynthesis.[3, 4] In molecular magnetism, manganese and iron ion assemblies with high nuclearities and appropriate topologies can sometimes possess large ground spin (S) values, and can function as single-molecule magnets (SMMs).[5-8] Such SMM displays slow relaxation of its magnetization and functions as a magnet below its so-called blocking temperature (T_B).[9-11] While at low temperatures quantum tunnelling becomes the dominant relaxation path for the magnetization, a thermally activated regime dominated mainly by the spin ground state (S_T) and the uni-axial anisotropy (D) of the molecule is observed at higher temperatures. In this regime, the theoretical energy barrier (Δ) is equal to $|D|S_T^2$ or $|D|(S_T^2 - 1/4)$ for integer and half-integer S_T, respectively. Thus it is important to find molecules exhibiting large spins and/or large D values. Mn(III) ions, having a d^4 ground state and negative magnetic anisotropy, are perfect candidates for development of molecular magnetic materials. The high spin iron(III) ion (d^5), having an S = 5/2 ground state, is also a potential building block to achieve large spin in the ground state, but due to its ^6S nature, it generally forms antiferromagnetically coupled clusters.[12, 13] However, certain Fe_x topologies have resulted in large ground spin states, due to the occurrence of the spin frustration effects, showing slow magnetic relaxation and magnetic hysteresis.[14, 15] A major obstruction to the practical application of these nanomagnets is the low blocking temperatures up to which the molecule behaves as a nanomagnet. Although many efforts have been made to increase Δ and τ, the first family of SMMs, $[Mn_{12}O_{12}(OR)_{12}(H_2O)_4]$ still displays the highest blocking temperatures of all the complexes studied so far.[11, 16, 17] A major goal in the development of new nanomagnets is to develop ligands that give rise to novel clusters in

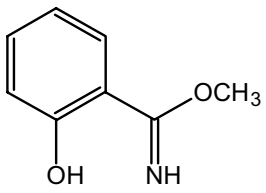

Figure 5.1: The ligand methyl salicylimidate

order to rationalize the geometry, nuclearity and topologies of Mn, Fe clusters. Through the development of new varieties of SMMs high blocking temperatures could be achieved, which would permit their use as in actual applications.

During the studies on new epoxidation catalysts based on manganese complexes, the ligand methyl salicylimidate (HMesalim) (Figure 5.1) has proven to be a useful synthetic intermediate. The coordination chemistry of the ligand appears to be very rich, and recently crystal structures of three manganese complexes, as well as their catalase activities have been published (see chapter 2).[18, 19] In this chapter, the syntheses, X-ray crystal structures and detailed magnetic properties of three novel high nuclearity manganese and iron complexes, $[Mn_6O_4(OMe)_2(OAc)_4(Mesalim)_4]$ (**3**), $[Mn_8O_2(OH)_2(OMe)_{12}(OAc)_2(Mesalim)_4]$ (**4**) and $[Fe_{10}O_4(OMe)_{14}Cl_2(Mesalim)_6]$ (**5**) are reported.

5.2 Experimental Section

5.2.1 Physical measurements

UV/Vis-NIR measurements were performed on a Perkin-Elmer Lambda 900 UV/Vis/NIR spectrometer. IR spectra were recorded on a Perkin-Elmer FT-IR Paragon 1000 spectrometer. Elemental analyses were performed with a Perkin-Elmer series II CHNS/O analyzer 2400. Magnetic measurements were done with a Quantum Design MPMS-XL squid magnetometer on slightly powdered polycrystalline samples. Corrections for the sample holder (empirically determined) and intrinsic diamagnetism (Pascal constants) of the samples were applied. All solvents were of analytical grade and used without further purification unless stated otherwise. The ligand HMesalim was synthesised according to the reported procedure.[20-22] Synthesis of the complex $[Mn(Mesalim)_2(OAc)(MeOH)]\cdot MeOH$ (**1**) has been described in chapter 2.[19]

5.2.2 Syntheses

$[Fe(Mesalim)_2Cl]$ (**2**): To a solution of 0.1 g (0.662 mmol) HMesalim, in 5 mL CH_3CN-MeOH (50:50 v/v) mixture, 0.054 g (0.332 mmol) of solid $FeCl_3$ was added in a 5 mL CH_3CN-MeOH (50:50 v/v) mixture. The resulting purple-red solution was stirred for 30 minutes. The solution was filtered and crystals suitable for X-ray analysis were obtained by slow diffusion of a mixture of hexane/Et_2O (1:1, v/v) into the reaction mixture. Yield of crude product: 61% (0.08 g); IR (diamond): 3308(m), 3023(s), 1614(s), 1587(m), 1538(vs), 1452(m), 1435(m), 1385(s), 1329(s), 1261(s), 1204(s), 1157(m), 1099(s), 1033(s), 960(s), 864(s), 788(m), 750(vs), 665(m), 629(m), 563(s), 528(s), 481(s), 435(s) cm^{-1}; Elemental

analysis calc (%) for $C_{16}H_{16}ClFeN_2O_4$ (FW = 391.61): C, 49.07; H, 4.12; N, 7.15. Found: C, 49.00; H, 4.51; N, 7.26

$[Mn_6O_4(OMe)_2(OAc)_4(Mesalim)_4]$ (**3**): To a solution of 0.2 g (1.32 mmol) HMesalim in 5 mL MeOH, a solution of 0.486 g (1.98 mmol) Mn(II) acetate in 5 mL MeOH was added. The resulting brown solution was stirred for 30 minutes at 50 °C. The solution was filtered, and crystals suitable for X-ray analysis were obtained by slow diffusion of a hexane/Et_2O(1:1 v/v) mixture into the reaction mixture. Yield of crude product: 23% (0.1 g); The complex **3** could also be obtained by slow diffusion of a solution of the complex $[Mn(Mesalim)_2(OAc)(MeOH)]\cdot MeOH$ (**1**) in MeOH with Et_2O. However, the complex **3** obtained with this route was impure, as observed from the elemental analyses. IR (diamond): 3268(m), 1606(s), 1588(s), 1455(s), 1399(s), 1214(m), 1088(vs), 959(m), 868(m), 758(s), 618(s), 523(s), 427(s) cm^{-1}; Elemental analysis calc (%) for $C_{27}H_{31}MnN_{30}O_{10}$ (FW = 1295.88): C, 50.05; H, 4.82; N, 6.4. Found: C, 50.0; H, 5.07; N, 6.67

$[Mn_8O_2(OH)_2(OMe)_{12}(OAc)_2(Mesalim)_4]$ (**4**): The complex $[Mn(Mesalim)_2(OAc)(MeOH)]$ (0.5 g) was dissolved in MeOH (250 ml), and the solution was filtered. The solution was kept in a 250 ml conical flask with a stopper and allowed to stand for 2-3 months. Brown crystals suitable for X-ray analysis were obtained in a very low yield. The brown crystals were the sole product isolated from the solution. Despite the low yields the complex has been reproduced several times. Yield of crude product: ~ 5% (10 mg); IR (diamond): 2907(m), 2809(s), 1616(s), 1550(s), 1544(s), 1452(m), 1397(vs), 1336(m), 1266(m), 1211(s), 1158(s), 1139(s), 1063(s) 1035(m), 866(s), 756(s), 866(s), 635(s), 550(m), cm^{-1}; Elemental analysis calc (%) for $C_{48}H_{76}Mn_8N_4O_{28}$ (FW = 1596.65): C, 36.1; H, 4.8; N, 3.5. Found: C, 35.88; H, 4.61; N, 3.50.

$[Fe_{10}O_4(OMe)_{14}Cl_2(Mesalim)_6]$ (**5**): Complex **2** (20 mg) was dissolved in ~ 10 mL MeOH, and the covered solution was left to stand for 1-2 months. The purple solution turned orange over time and gave small orange crystals suitable for X-ray analysis. Yield of crude product: 70% (7 mg); IR (diamond) 3302(m), 2915(m), 2814(m), 1618(s), 1546(w), 1470(m), 1449(s), 1389(s), 1326(s), 1262(s), 1202(s), 1153(s), 1096(m), 1048(vs), 869(m), 785(w), 751(s), 668(m), 599(s) 457(m), 460(m), 394(m) cm^{-1}; Elemental analysis calc (%) for $C_{62}H_{90}Cl_2Fe_{10}N_6O_{30}\cdot 4H_2O$ (FW = 2028.78): C, 35.45; H, 4.70; N, 4.00. Found: C, 35.55; H, 4.94; N, 3.84.

5.2.3 X-ray Crystallographic Study

$[Mn_6O_4(OMe)_2(OAc)_4(Mesalim)_4]$ (**3**), $[Mn_8O_2(OH)_2(OMe)_{12}(OAc)_2(Mesalim)_4]$ (**4**) and $[Fe_{10}O_4(OMe)_{14}Cl_2(Mesalim)_6]$ (**5**): Data on measurement and structure determination are presented in Table 5.1. Intensity data for **3**, **4** and **5** were collected at 150 K on a Nonius Kappa CCD diffractometer with rotating anode (Mo K_α, λ = 0.71073 Å). A multi-scan absorption correction was applied to each data set using PLATON/MULABS.[23] The structures were solved by direct methods using SHELXS97, and refined on F^2 using SHELXL97.[24] Crystal structures **3** and **5** contain voids (453.9 $Å^3$/unit cell for **3**; 106.9 $Å^3$/unit cell for **5**) filled with disordered methanol solvent molecules. Their contribution to the structure factors was ascertained using PLATON/SQUEEZE (106 e/unit cell for **3**; 15 e/unit cell for **5**).[23] All non-hydrogen atoms were refined with anisotropic displacement parameters. The imine hydrogen atoms were positively identified in a difference Fourier map. All hydrogen atoms were constrained to idealized geometries and allowed to ride on their carrier atoms with an isotropic displacement parameter related to the equivalent displacement parameter of their carrier atoms. The H atom of the H-bonded systems O3···O112 and O4···O114 in complex **4** has been arbitrarily assigned to the μ_3–O atom rather than the μ–OCH_3 atom. Structure validation and molecular graphics preparation were performed with the PLATON package.[23].

5.3 Results and Discussion

5.3.1 Synthetic Aspects

The various polynuclear clusters described in this chapter were mainly obtained by recrystallization of mononuclear complexes under a variety of conditions. The mononuclear complexes were obtained from straightforward synthetic procedures. The reaction of HMesalim with manganese(II) acetate in a 2:1 ratio in a methanol/ether mixture yields the mononuclear complex $[Mn(Mesalim)_2(OAc)(MeOH)]\cdot MeOH$ (**1**), the crystal structure of which is discussed in chapter 2.[19] In a similar way, the reaction of HMesalim with iron(III) chloride in a 2:1 ratio in a THF/methanol mixture gives the mononuclear complex $[Fe(Mesalim)_2Cl]$ (**2**), the composition of which has been confirmed by elemental analysis, IR and ESI-MS analyses.

Recrystallization of complex **1** resulted in the formation of the two novel clusters $[Mn_6O_4(OMe)_2(OAc)_4(Mesalim)_4]$ (**3**) and $[Mn_8O_2(OH)_2(OMe)_{12}(OAc)_2(Mesalim)_4]$ (**4**). Complex **1**, when recrystallized from a bilayer system of methanol/hexane+diethyl ether (1:1

v/v), gives brown crystals of complex **3** as confirmed by X-Ray diffraction analysis. Thus, complex **3** may have been formed by hydrolysis of complex **1** with water and methanol as summarized in Eq. 1.

$$6\,[Mn(Mesalim)_2(MeOH)(OAc)] + 4\,H_2O \rightarrow [Mn_6O_4(OMe)_2(OAc)_4(Mesalim)_4] + 8\,HMesalim + 4\,AcOH + 4\,MeOH \quad (1)$$

Complex **3** has also been synthesized directly in very good purity and yield by the reaction of HMesalim with manganese(II) acetate in a 2:3 ratio (Eq. 2).

$$6\,Mn(OAc)_2 + 4\,HMesalim + 2MeOH + 3H_2O + O_2 \rightarrow [Mn_6O_4(OMe)_2(OAc)_4(Mesalim)_4] + 8\,AcOH + 4\,MeOH \quad (2)$$

It is possible that the extra oxidizing equivalents necessary for the oxidation of the Mn(II) ions to Mn(III) ions originate from atmospheric dioxygen, or from oxidation products of solvent or ligand groups. Water was readily available in the solvent, which was not distilled. Complex **4** was obtained by very slow evaporation of complex **1** from a dilute methanol solution over a period of a few months in a yield of ~ 5%. (Eq 3)

$$8\,[Mn(Mesalim)_2(MeOH)(OAc)] + 4\,H_2O \rightarrow [Mn_8O_2(OH)_2(OMe)_{12}(OAc)_2(Mesalim)_4] + 12\,HMesalim + 6\,AcOH \quad (3)$$

Despite the low yields and longer times necessary for the crystallization, complex **4** can be readily reproduced. Unlike complex **3**, complex **4** could not be synthesized directly by reaction of the metal and ligand in a ratio of 2:1, as present in the complex, or by the use of sodium methoxide as a source of the methoxide ions. Instead, the IR of the crystalline products obtained under the above conditions showed the characteristic vibrations for both the complexes **3** and **4**, suggesting that a mixture of the two complexes had formed. The isolation of complex **3** together with complex **4** rather than the pure complex **4,** in reactions with metal to ligand ratios of 2:1 (similar to that in complex **4**), or under different conditions, suggests that **3** might be the kinetic product of the reaction while **4** is the thermodynamic product. By controlling the solvents used for recrystallization, the two different clusters from the same reaction mixture have been isolated in pure and crystalline form. The formation of

manganese clusters from their mononuclear five- or six-coordinate complexes, with other counter-ions, such as chloride or bromide, has been demonstrated previously.[25] However, recrystallization of the other mononuclear and dinuclear manganese complexes of the ligand HMesalim, $[Mn(Mesalim)_2Cl]$[18] and $[Mn_2(Etsalim)_4(HEtsalim)_2](ClO_4)_2]$[19] (HEtsalim = ethyl salicylimidate), did not yield any polynuclear species, even after several months, as observed from the ESI-MS analysis of the solutions. In contrast, slow evaporation of a methanolic solution of the complex $[Fe(Mesalim)_2Cl]$ (**2**) over a period of 2-3 months resulted in the formation of the decanuclear cluster $[Fe_{10}O_4(OMe)_{14}Cl_2(Mesalim)_6]$ (**5**). The overall reaction occurring in solution can be summarized as given in Eq 4.

$$10\ [Fe(Mesalim)Cl] + 4\,H_2O + 14\,MeOH \rightarrow [Fe_{10}O_4(OMe)_{14}Cl_2(Mesalim)_6] + 8\,HCl + 14\,HMesalim \quad (4)$$

Reaction of the ligand and $FeCl_3$ in a ratio of 3:5, as in the complex, did not result in the formation of complex **5**. Reaction of metal salts with the ligand in appropriate ratios or use of sodium methoxide as a source of methoxide ions are commonly used methods for the synthesis of oxo/methoxo-bridged, polynuclear manganese or iron complexes. These methods, however, proved unsuccessful for the direct synthesis of complexes **4** and **5** in the present work.

5.3.2 Description of the Crystal Structures

A PLUTON representation of the molecular structure of **3** is shown in Figure 5.2. A PLUTON projection of the core of the molecule is shown in Figure 5.5A. Structural data and details of the data collection and refinement are summarized in Table 5.1. Selected bond distances are summarized in Table 5.2. Selected bond angles are summarized in Appendix A3; Table 1, at the end of this thesis.

The molecule can be regarded as being built from a face-sharing double-cubane cluster with an $[Mn_6O_6]$ core. It is located on a crystallographic inversion center. It consists of six Mn(III) cations, two μ_4-O^{2-} anions, two μ_3-O^{2-} anions, two μ_3-OMe^- anions, four OAc^- anions and four terminal anionic Mesalim ligands. The centrosymmetric complex comprises two groups of Mn_3 clusters, and can alternatively be interpreted as a dimer of trimers joined together by oxide, methoxide and carboxylate bridges. Based on charge considerations, all six manganese centers can be assigned as manganese(III), which is confirmed by the elongated octahedral geometries observed for each six-coordinate manganese ion, as is typical for Jahn–

Teller distorted d^4 systems. The four peripheral manganese ions are in an NO_5 coordination environment, whereas the two central manganese ions have O_6 chromophores.

Together with two μ_4-oxide bridges, the two central manganese ions form the shared face between the two cubes. The two central μ_4-oxides are each coordinated to two manganese ions at the corners of the double-cubane, in addition to the central manganese

Table 5.1: Crystal data for complex **3**, **4** and **5**

	3	**4**	**5**
Formula[a]	$C_{42}H_{50}Mn_6N_4O_{22}$	$C_{48}H_{76}Mn_8N_4O_{28}$	$C_{62}H_{90}Cl_2Fe_{10}N_6O_{30}$
Fw, g/mol[a]	1292.50	1596.65	2028.80
crystal System	Triclinic	Monoclinic	Triclinic
space group	P-1 (No. 2)	P21/c (No. 14)	P-1 (No. 2)
a, Å	10.3718(2)	9.753(3)	10.7152(3)
b, Å	11.8762(3)	27.559(6)	12.7086(3)
c, Å	13.4373(3)	25.860(8)	16.3521(6)
α, deg	78.6455(8)		110.1462(11)
β, deg	79.7779(8)	115.621(13)	101.8144(11)
γ, deg	79.5352(9)		92.868(2)
V, Å^3	1578.46(6)	6267(3)	2028.54(11)
Z	1	4	1
ρ_{calc}, g/cm$^{3\,a}$	1.360	1.692	1.661
μ, mm$^{-1\,a}$	1.231	1.643	1.879
[*T*, K]	[150]	[150]	[150]
Transmisson range	0.841- 0.979	0.787 – 0.880	0.822 – 0.948
Total reflections	24397	95838	23629
Unique reflections	6182	11344	7128
Parameters	339	811	496
wR2	0.0971	0.1582	0.1155
*R*1 *[*(I)> 2σ (I)]	0.0395 (4579 refl.)	0.0816 (5644 refl.)	0.0471 (4927 refl.)
S	1.05	1.06	1.05

[a] Where relevant, without disordered solvent contribution

Table 5.2: Selected bond distances (Å) for complex **3**. Symmetry code: a: –x, –y, 2–z.

Mn1–O1	1.9471(17)	Mn2–N39	1.979(2)
Mn1–O2	1.9269(17)	Mn2–O2_a	1.9586(17)
Mn1–O17	1.8788(18)	Mn3–O1	1.8827(17)
Mn1–O52	2.1441(19)	Mn3–O2	2.3958(18)
Mn1–O71	2.2811(18)	Mn3–O53	1.9338(18)
Mn1–N19	1.986(2)	Mn3–O63	2.1507(18)
Mn2–O1	1.9172(18)	Mn3–O2_a	1.9357(17)
Mn2–O37	1.8632(18)	Mn3–O71_a	1.9016(18)
Mn2–O71	2.3715(18)	Mn2–O62	2.1632(19)

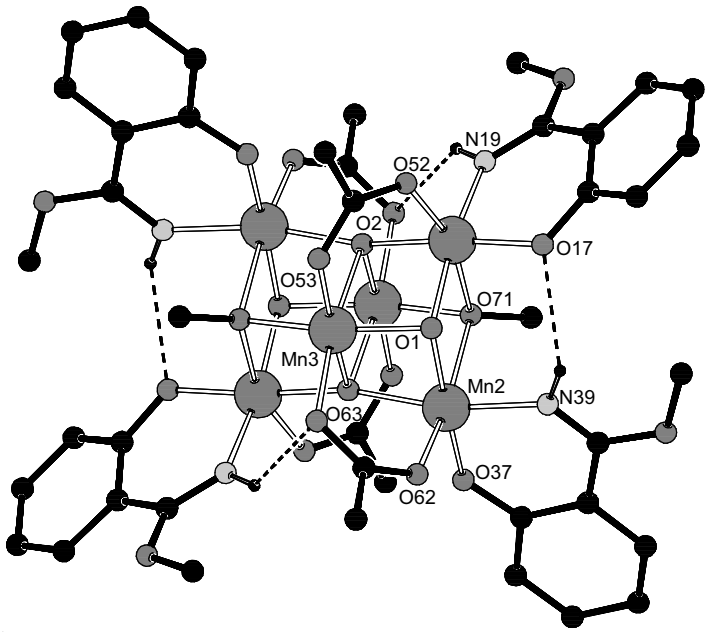

Figure 5.2: PLUTON representation of the molecular structure of **3**. Hydrogen atoms not involved in hydrogen bonding are omitted for clarity.

ions, in an unusual "sawhorse" geometry. At each outer face of the double-cubane, two manganese ions are bridged by a μ_3-methoxide group and a "normal sp^3 type" μ_3-oxide. Each of the peripheral manganese ions is connected to a third, central manganese ion, via a bridging carboxylate group.

Finally, the octahedral coordination environment of the peripheral manganese ions is completed by coordination of the didentate Mesalim ligand, in such a way that for Mn1 the imine nitrogen is *trans* to a μ_3-oxide, while for Mn2 the imine nitrogen is *trans* to a μ_4-oxide. Thus, Mn1 and Mn2 are each coordinated by one μ_4-oxide, one μ_3-oxide, one μ_3-methoxide, one bridging carboxylate group and one didentate Mesalim ligand. The coordination sphere of the central Mn3 comprises two μ_4-oxides, one μ_3-oxide, one μ_3-methoxide and two bridging carboxylate groups. The Jahn–Teller axes of the peripheral manganese ions Mn1 and Mn2 lie along the line from the carboxylate oxygen to the μ_3-methoxide, avoiding the oxygen or nitrogen from the ligand, and are therefore perpendicular to each other. The Jahn–Teller axis of the Mn3 ion, which is along O2–Mn3–O63, is parallel to that of Mn2 (along O62–Mn2–O71). Two types of hydrogen bonds are present within the cluster (Figure 5.2). Details of the hydrogen bonding interactions are summarized in Table 5.5. The imine group of the Mesalim ligand coordinated to Mn2 forms a hydrogen bond with the phenolate oxygen

Table 5.3: Selected bond distances for complex **4**

Mn1–O3	1.933(6)	Mn3–O124	2.163(7)
Mn1–O17	1.862(7)	Mn3–O126	1.883(5)
Mn1–O93	2.217(8)	Mn3–O130	2.150(6)
Mn1–O122	2.236(7)	Mn5–O1	1.967(6)
Mn1–O124	1.923(6)	Mn5–O2	2.305(5)
Mn1–N19	1.996(8)	Mn5–O4	1.952(6)
Mn2–O1	2.295(5)	Mn5–O128	2.249(5)
Mn2–O2	1.957(6)	Mn5–O130	1.886(6)
Mn2 –O3	1.952(6)	Mn5–O132	1.895(6)
Mn2–O122	1.889(7)	Mn7–O1	1.911(5)
Mn2–O138	2.260(5)	Mn7–O57	1.885(6)
Mn2–O140	1.881(6)	Mn7–O114	2.331(7)
Mn3–O1	2.000(6)	Mn7–O126	2.273(6)
Mn3–O3	1.907(5)	Mn7–O128	1.916(6)
Mn3–O94	2.012(7)	Mn7–N59	2.000(8)

of the neighboring Mesalim coordinated to Mn1 (N39···O17 = 3.091(3) Å). The imine group of the Mesalim ligand bound to Mn1 forms a hydrogen bond with an adjacent carboxylate oxygen (N19···O63a = 3.200(3) Å).

A PLUTON representation of the molecular structure of **4** is shown in Figure 5.3. A PLUTON projection of the core of the molecule is shown in Figure 5.5B. Selected bond distances are summarized Table 5.3. Selected bond angles are summarized in Appendix A3; Table 2, at the end of this thesis.

Structural analysis of the complex **4** shows the compound to consist of neutral octanuclear clusters, containing eight Mn(III) ions, two μ_4-O^{2-}, two μ_3-OH^-, ten μ-OMe^-, two terminal OMe^-, two OAc^- anions and four terminal anionic Mesalim ligands. An alternative description of the complex would involve two terminal MeOH instead of OMe^- and two O^{2-} instead of OH^-. These descriptions differ only in the position of two H atoms. These H atoms are most likely disordered and could not be located on difference Fourier maps.

The molecule has non-crystallographic inversion symmetry (RMS deviation 0.109 Å). All manganese ions are in a pseudo-octahedral environment. The four peripheral ones (Mn1, Mn4, Mn7 and Mn8) are in an NO_5 coordination sphere, whereas the four central manganese ions (Mn2, Mn3, Mn5 and Mn6) have MnO_6 chromophores. Complex **4** can be described as consisting of six $[Mn_3O_4]$ partial cubane units that are commonly encountered in high nuclearity manganese compounds, the two central units sharing one face. Furthermore, each of the central partial cubane units shares a face with two of the four remaining units. The two terminal MeO^- ions, the bridging acetates and the anionic Mesalim ligands are not involved

in the formation of partial cubanes, and complete the coordination sphere around the manganese ions. Pairs of neighbouring manganese ions are connected by two O bridges, the exception being the Mn1–Mn3 pair, and its pseudo-symmetrical counterpart Mn4–Mn6 pair, which have an additional acetate bridge resulting in shorter Mn….Mn separation (2.94 Å). In addition, the Mn2–Mn7 and Mn5–Mn8 pairs are connected by a single unique asymmetric μ_4-O^{2-} bridge (For Mn2–Mn7 pair; Mn–O of 2.295(5) and 1.911(5) Å, Mn–O–Mn = 150.7(3)° , For Mn5–M8, Mn–O of 2.305(5) and 1.921(5) Å, Mn–O–Mn = 150.8(3)°) resulting in a longer Mn….Mn separation (4.070(2) Å). All Mn(III) ions present elongated JT axes, which is known to result in a negative value of the axial zero field splitting parameter.[26] In the central Mn2–Mn5 pair both bridging O atoms lie along the JT elongation axis of either of the Mn ions, the JT axes of the two Mn(III) ions being parallel with each other in this case (Figure 5.5B) (short Mn–O bond, 1.957(6) and 1.967(6) Å, long Mn–O bond, 2.295(5) and 2.305(5) Å, Mn2…Mn5 = 3.248(2) Å). In contrast, in the rest of the pairs (Mn…Mn separations of 3.02 to 3.09 Å) only one of the two bridging O atoms lies on JT axis of one of the manganese ions resulting in the orthogonality of the JT axes. The JT axes of Mn1, Mn4, Mn7 and Mn8 are all parallel to each other; the JT axis of Mn2 is parallel to Mn5 while the JT axis of Mn3 is parallel to Mn6. Each of the above three groups of parallel JT axes are approximately orthogonal to the other two orientations. A resulting significant magnetic anisotropy can thus be expected. Remarkably, the outer manganese ions do not have their JT axes along the bonds to ligand oxygen or nitrogen atoms. Three types of hydrogen bonds are present within the cluster (Figure 5.3). Details of the hydrogen bonding interactions are summarized in Table 5.5. The imine group of the Mesalim ligand coordinated to Mn1, Mn8, Mn4 and Mn7 form a hydrogen bond with the methoxo oxygen coordinated to Mn8, Mn4, Mn7 and Mn1 each respectively (D–H…A = 2.931(9) -3.064(8)). In addition, as discussed above, the methoxo oxygen, O112 coordinated to Mn8 forms a hydrogen bond with the hydroxo oxygen, O3 coordinated to Mn1, and similar description would apply to the symmetric counterpart of the molecule (O114….O4). As these H atoms are most likely disordered and could not be located on difference Fourier maps, it cannot be confirmed if the hydrogen atom exists as a proton on a methanol molecule attached to the manganese or a proton coordinated to oxygen as a hydroxo group.

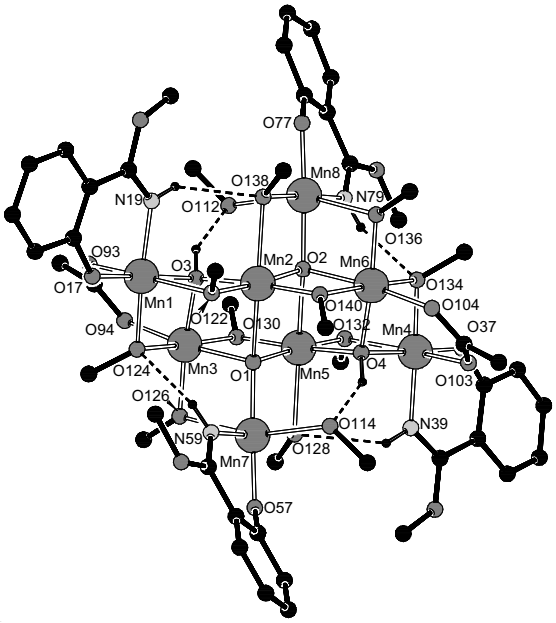

Figure 5.3:PLUTON representation of the molecular structure of **4**. Hydrogen atoms not involved in hydrogen bonding are omitted for clarity

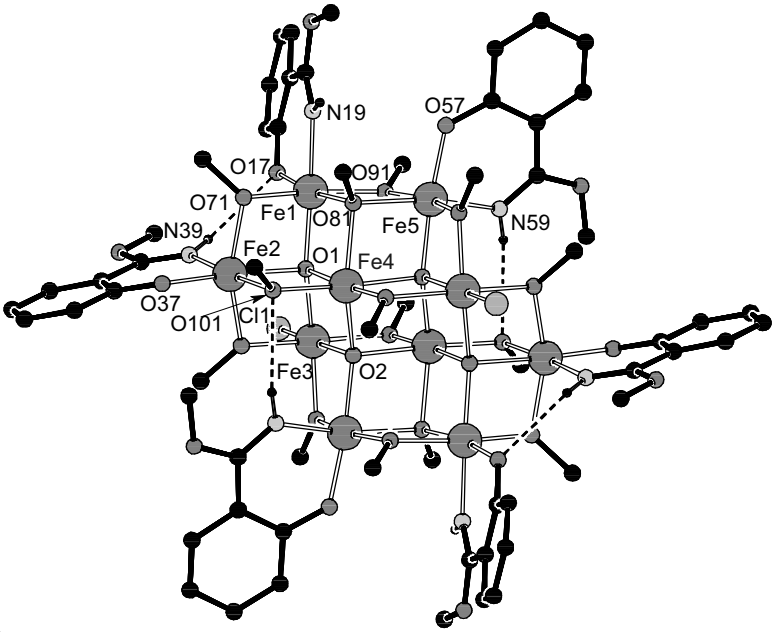

Figure 5.4: A PLUTON representation of the molecular structure of **5**. Hydrogen atoms not involved in hydrogen bonding are omitted for clarity.

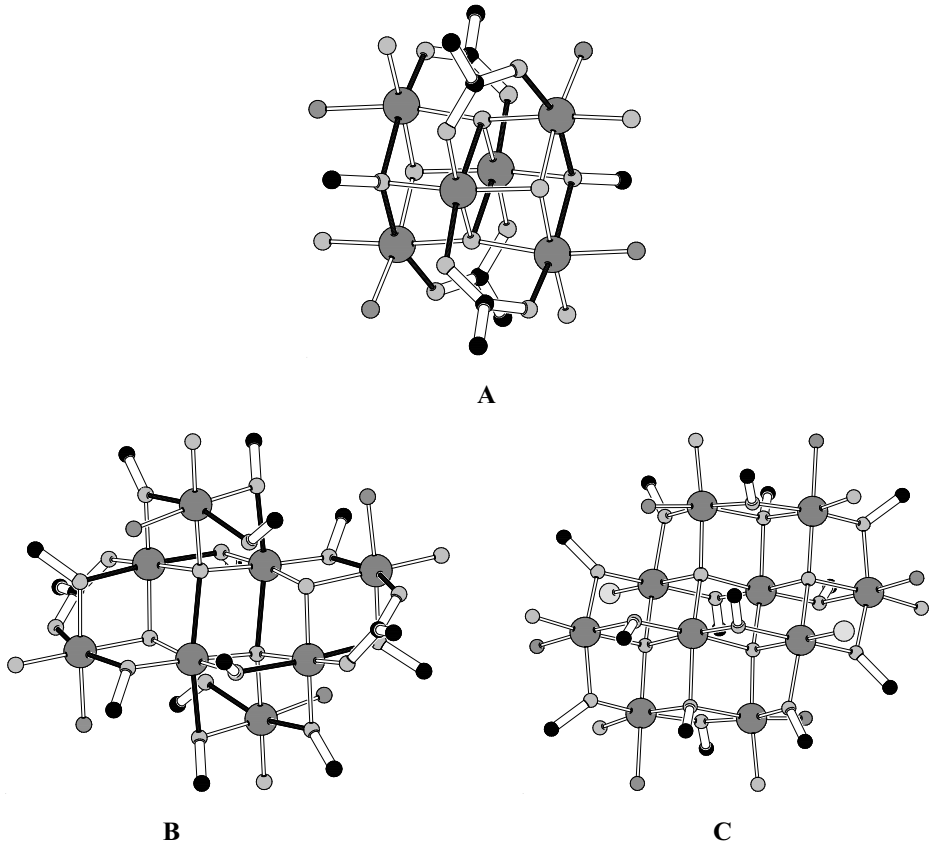

Figure 5.5: PLUTON projections of the cores of complexes **3** $[Mn_6O_6]$ (A), **4** $[Mn_8O_{14}]$ (B) and **5** $[Fe_{10}O_{18}]$ (C). The bold lines in figures A and B depict JT axes for the Mn(III) ions.

A PLUTON projection of the molecular structure of complex **5** is shown in Figure 5.4 and a PLUTON projection of the core of the molecule is shown in Figure 5.5C (right). Selected bond distances are summarized in Table 5.4 and selected bond angles are given in Appendix A3; Table 3, at the end of this thesis. The molecule consists of ten Fe(III) cations, four μ_4-O^{2-} anions, two μ_3-OMe^- anions, twelve μ-OMe^- anions, two Cl^- anions and six terminal anionic Mesalim ligands. The molecule is located on a crystallographic inversion center. There are four different types of distorted octahedral coordination environments for the five iron ions in the asymmetric unit, $[Fe(\mu\text{-}OMe)_3(\mu_4\text{-}O)(L)]$, $[Fe(\mu\text{-}OMe)_2(\mu_3\text{-}OMe)(\mu_4\text{-}O)(L)]$, $[Fe(\mu\text{-}OMe)_2(\mu_3\text{-}OMe)(\mu_4\text{-}O)_3]$ and $[Fe(\mu\text{-}OMe)_3(\mu_4\text{-}O)_2Cl]$. The phenolate oxygen donors of the ligands are bound more tightly to the iron centers than the other coordinating oxygen ions. Thus, Fe1–O17, Fe2–O37 and Fe5–O57 bond distances are 1.921(3) Å, 1.909(3) Å, and 1.922(3) Å, respectively, while the

Table 5.4: Bond distances for complex **5**. Symmetry code: a: 1–x, –y, 1–z.

Fe1–O1	1.970(3)	Fe3–O101	2.014(3)
Fe1–O17	1.921(3)	Fe3–O121	2.052(3)
Fe1–O71	2.016(3)	Fe3–O131	1.998(3)
Fe1–O81	2.118(3)	Fe4–O1	2.082(3)
Fe1–O91	1.988(3)	Fe4–O2	1.944(3)
Fe1–N19	2.098(3)	Fe4–O81	2.119(3)
Fe2–O1	2.081(3)	Fe4–O111	1.998(3)
Fe2–O37	1.909(3)	Fe4–O2_a	2.066(2)
Fe2–O71	2.002(3)	Fe4–O121_a	1.970(3)
Fe2–O101	1.976(3)	Fe5–O2_a	1.988(2)
Fe2–O111	2.064(3)	Fe5–O57	1.923(3)
Fe2–N39	2.106(3)	Fe5–O131_a	2.006(3)
Fe3–Cl1	2.3064(12)	Fe5–N59	2.067(3)
Fe3–O1	2.017(3)	Fe5–O81	2.119(3)
Fe3–O2	2.099(2)	Fe5–O91	2.014(3)

Table 5.5: Hydrogen bond donor acceptor distances for complexes **3**, **4** and **5**. Symmetry codes: a: –x, –y, 2–z; b: 1–x, –y, 1–z.

3		**4**		**5**	
N19--H19 O63a	3.200(3)	O3-- H3 O112	2.643(9)	N39--H39 O17	3.143(5)
N39--H39 O17	3.091(3)	O4-- H4 O114	2.658(9)	N59-- H59 O111b	3.399(5)
		N19-- H19 O138	2.940(9)		
		N39--H39 O128	3.064(8)		
		N59--H59 O124	2.994(10)		
		N79--H79 O134	2.931(9)		

other Fe–oxo distances lie in the range of 1.943(3)–2.119(3) Å. Pairs of closest iron neighbors are connected by two methoxo or oxo bridges. The distance between the iron ions is dependent on the bridging ligands, and decreases in the order 2 μ-methoxo (3.2099(9) Å) > 1 μ-methoxo and 1 μ-oxo (range 3.0531(9) – 3.1485(8) Å) > two μ-oxo (3.0680(9) Å).

There are two intramolecular hydrogen bonds present in the asymmetric unit of the complex (Figure 5.4, Table 5.5), one is formed by hydrogen bonding between the imine nitrogen of one of the Mesalim ligands and one of the methoxo bridges, and the other is formed between the imine nitrogen of one of the Mesalim ligands and the phenoxo oxygen of a neighboring Mesalim ligand. One of the N-H groups does not donate an H-bond. The $[Fe_{10}O_{18}]$ core of complex **5** can be described as consisting of ten $[Fe_3O_4]$ partial cubane units, the outer eight being doubly face-sharing and the central two being triply face-sharing.

5.3.3 Discussion of the Crystal Structures

Complex **3** contains an isolated face-sharing double cubane core that is rare in manganese or iron cluster chemistry. The $[M_2O_4]$ (butterfly), $[M_3O_4]$ (partial cubane), and $[M_4O_4]$ (cubane), $[M_4O_6]$ (adamantane) are commonly occurring subunits in high nuclearity manganese and iron clusters. Face-sharing double cubane subunits are commonly found in the polyoxo-molybdate or -vanadate chemistry, [27-29] and are found in few manganese and iron clusters.[30-32]

Isolated, well-defined face-sharing double cubane $[M_6O_6]$ units are only found in a few sodium[33, 34], potassium[35] and calcium[36] complexes. The isolated $[Mn_6O_6]$ core of complex **3** is the first to be observed in a transition metal oxide cluster.

Interestingly, a mixed metal $Ru_4Mo_4O_{16}$ cluster has been studied by multinuclear NMR by Artero et al, and it has been shown to exist in solution as two isomers, the windmill-like form (similar to complex **4**) and a triple-cubane form (similar to complex **3**), while the double cubane cluster $Ru_4W_2O_{10}$, was found to be formed as a byproduct of the synthesis of the windmill like cluster $Ru_4W_4O_{16}$.[37] In the course of the synthesis of complexes **3** and **4**, it was found that by changing the M:L ratio from 1:3 to 2:1 or 2:3, a crystalline product was obtained, the IR of which pointed to the possibility of mixture of the different clusters. However, by changing the solvents for crystallization the two clusters have been successfully isolated. The $[M_3O_4]$ unit observed in complexes **4** and **5** is a sub-fragment that is commonly encountered in high nuclearity manganese and iron clusters. However, it is also worth noting that octanuclearity in purely Mn(III) oxo/carboxylato compounds is quite rare,[15, 38-41] and the core present in **4** has not been reported so far. However, the central Mn_6 core in complex **4** and Fe_6 core in complex **5** resembles that of the hexamanganese complex reported by Tuchagues et al.[42] The structures of complexes **4** and **5** are very similar to each other. In fact, it can be easily visualized that the $[Mn_8O_{14}]$ core of complex **4** can be derived from the $[Fe_{10}O_{18}]$ core of complex **5** by removal of two metal atoms, Fe5 and Fe5a, and four oxygen atoms. The structures of complexes **4** and **5** are also very similar to that of the heptanuclear manganese cluster $[Mn_7(OMe)_{12}(dbm)_6]$.[43] The difference is that complexes **4** and **5** contain three close-packed layers of oxygen atoms and two layers of metal atoms, as compared to two close-packed layers of oxygen atoms and a single layer of manganese atoms in the heptanuclear cluster.

Three complexes with the $[Fe_{10}O_{18}]$ core similar to that of complex **5** have been reported in literature: $[Fe_{10}O_4(OMe)_{16}(dbm)_6]$ (Hdbm = dibenzoylmethane),[44]

$[Fe_{10}Cl_8O_4(OMe)_{14}(MeOH)_6]\cdot 2MeOH$,[45] and $[(HL)_{12}Fe_{10}Na_4(\mu_4\text{-}O)_4(\mu_3\text{-}OH)_2(dme)_2(EtOH)_2]\cdot 2dme\cdot 8EtOH$, H_3L = 4-tert-butyl-2,6-bis(hydroxymethyl)phenol and dme = 1,2-dimethoxyethane).[13] Structurally, the $[Fe_{10}O_{18}]$ cores of these molecules can be considered as fragments of an iron oxide (wustite) or hydroxide (lepidocrocite) phase: the oxygen atoms of the cores are arranged in cubic close-packed layers with the iron atoms occupying the octahedral interstices.[46] Another complex worth mentioning here is also a $Ti_{10}O_{32}$ cluster that is exactly analogous to the complex **5**.[47]

5.3.4 Magnetism

Variable temperature magnetic susceptibility data were collected on bulk polycrystalline samples of complexes **3, 4** and **5** under a magnetic field of 0.1 T. Plots of $\chi_M T$ and χ_M^{-1} vs. T are given in Figure 5.6A and Figure 5.6B for complex **3** and **5** respectively, where χ_M is the molar magnetic susceptibility. The value of $\chi_M T$ per $[Mn_6]$ in **3** drops from 12.9 $cm^3mol^{-1}K$ at 300 K to 0.23 $cm^3mol^{-1}K$ at 2 K, with an acceleration of the decrease below 200 K. The value at room temperature is slightly smaller than expected for an uncoupled $[Mn^{III}_6]$ cage with $g = 2$, while the decrease upon cooling reveals the presence of antiferromagnetic interactions within the cluster. Indeed, both plots follow a Curie-Weiss behavior above ca. 150 K, with $C = 17.78$ $cm^3mol^{-1}K$ and $\theta = -112$ K. The Curie constant is consistent with six Mn(III) ions with a g value of 1.98, while the negative Weiss constant indicates the presence of dominant antiferromagnetic interactions (of the order of $\theta/S^2 = 30$ K) between the spin carriers.

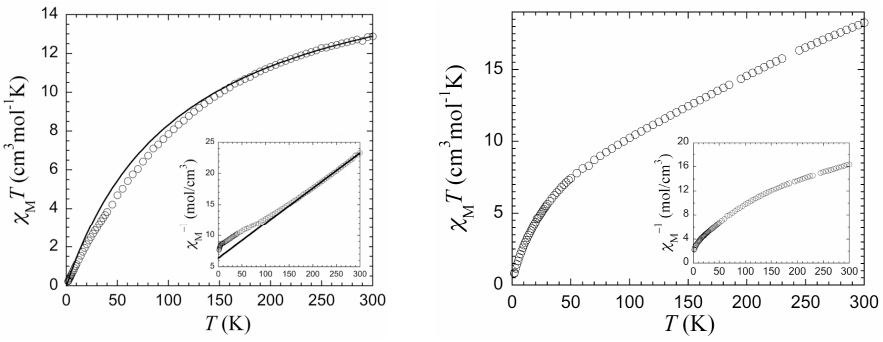

Figure 5.6: (A) Temperature dependence of the product $\chi_M T$ and χ_M^{-1} for **3** at 0.1 T. The solid lines represent the best fit to a Curie-Weiss law; **(B)** Temperature dependence of the product $\chi_M T$ and χ_M^{-1} for **5** at 0.1 T.

Below 150 K, the data deviate significantly from the Curie-Weiss law, suggesting that a magnetic model considering the different magnetic pathways within the $[Mn_6O_6]$ core should be used to analyze the low temperature data. *Syn-syn* axial acetate bridges are expected to couple the Mn(III) centers antiferromagnetically, while oxo and hydroxo bridges may yield weak ferromagnetic coupling, as in the well-known distorted cubane series $[Mn_4O_3X(O_2CR)_3(dbm)_3]$ (X = F^-, Cl^-, OH^-, etc.; R = Me, Et, Ph; dbm^- = the anion of dibenzoylmethane),[48] to moderate antiferromagnetic coupling. Although the geometry of the bridge (mainly the Mn–O–Mn angle) probably controls the exchange coupling, no correlation has been reported as yet in the literature with Mn(III). In addition, it was shown that even terminal ligands have to be considered because their influence on the energy of the metal *d* orbitals may change the energy difference with orbitals of the bridging ligand and therefore influence the strength of coupling.[11, 16] A quantitative analysis of the magnetic properties of **3** is thus complicated by the presence of five independent magnetic exchange interactions, whose pre-evaluation is not straightforward. In addition, the full magnetic coupling scheme has no analytical solution and would require the use of full-matrix diagonalization. At low temperatures (<50 K), zero-field splitting of the remaining S>1/2 states is also likely to take part in the sharper lowering of $\chi_M T$. Nevertheless, it can be concluded that the spin ground state of the Mn_6 cluster (complex **3**) is S_T = 0, as confirmed by magnetization *vs.* field measurements at 2 K that show extremely small values up to 7 T (Figure 5.7A).

Regarding complex **5**, the value of the product $\chi_M T$ at 300 K, 18.2 $cm^3mol^{-1}K$, is much lower than expected for 10 uncoupled Fe(III) S = 5/2 spins (43.75 $cm^3mol^{-1}K$ for g = 2), indicative of the presence of strong antiferromagnetic exchange interactions among the spin carriers. Indeed, $\chi_M T$ steadily decreases down to 8.05 $cm^3mol^{-1}K$ at 60 K, and further down to 0.82 $cm^3mol^{-1}K$ at 1.8 K. Oxo- and hydroxo-bridges such as those within the $[Fe_{10}O_{18}]$ core are expected to yield antiferromagnetic couplings of various strengths depending on their geometries,[1] and likely active even at 300 K, due to the high spin of Fe(III) ions. However, examination of the structure suggests that ten independent magnetic exchange interactions should be taken into account to model the behavior of complex **5**, precluding any simple analysis. Nevertheless, the observed behavior, with $\chi_M T$ tending to 0 at low temperatures, and the very low values of magnetization at 2 K, even at high fields (Figure 5.7B), point to a S_T = 0 ground state for the $[Fe_{10}]$ aggregate.

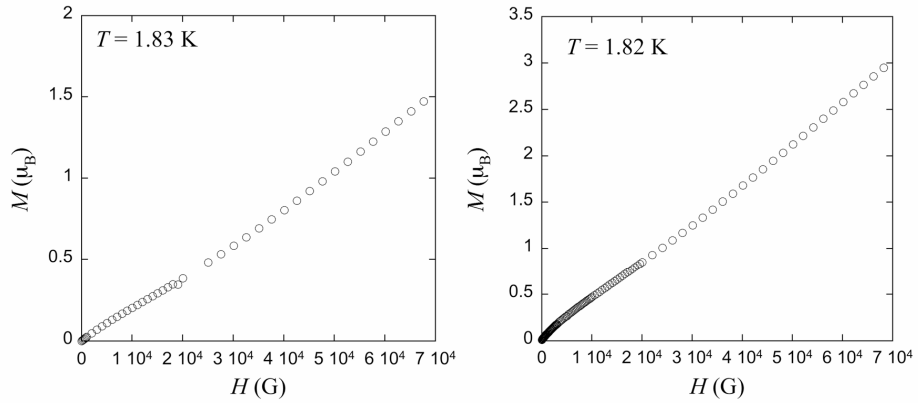

A **B**

Figure 5.7: (A) Magnetization vs. field data for complex **3** at 1.83 K. The small values of M at low fields are in agreement with a $S_T = 0$ ground state not fully populated at this temperature. The increase at the highest fields is likely due to the population of higher spin low-lying excited states; **(B)** Magnetization vs. field data for complex **5** at 1.82 K. The small values of M at low fields are in agreement with a $S_T = 0$ ground state not fully populated at this temperature. The increase at the highest fields is likely due to the population of higher spin low-lying excited states.

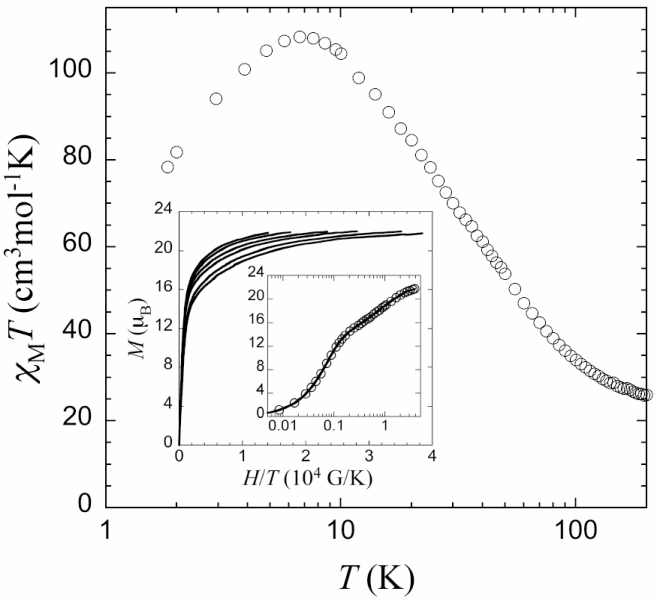

Figure 5.8: Plot of $\chi_M T$ *vs.* T under 0.1 T for complex **4**. Inset: Reduced magnetization data as normal and semilog plots.

Considering the moderate antiferromagnetic coupling observed in complex **3**, a mixed-valent species possessing the same $[Mn_6O_6]$ core might result in high spin molecules through non-compensated spins. This could possibly be achieved by electrochemical modification of the present cluster. In both complexes **3** and **5**, the occurrence of dominant antiferromagnetic interactions arises as a result of the geometry of the oxo- and hydroxo-bridges within the core of the clusters. Other geometries with different exchange interactions can also be obtained with the ligand HMesalim, which in all cases acts as an outer protective shell. Complex **4**, in which all the Jahn–Teller axes are parallel, is a good example.

In case of the complex **4**, the temperature dependence of $\chi_M T$ shown in Figure 5.8 indicates the presence of dominant ferromagnetic interactions among the $[Mn_8]$ core, yielding a high-spin ground state. The value of $\chi_M T$ at 300 K is in good agreement with the spin only value for eight uncoupled $S = 2$ spins, e.g. 24 cm^3Kmol^{-1}. (see Figure 5.8). Owing to the size of the molecule and the symmetry of the interaction scheme, it was neither possible to apply the Kambe method[49] nor a simple numerical approach to evaluate the exchange parameters between the Mn(III) ions. Nevertheless, the central Mn2–Mn5 interaction is expected to be ferromagnetic, as observed in such out-of-plane Mn(III) dimeric units,[50] while the other exchange parameters are likely to be much weaker, of either sign. The reduced magnetization plot presents a very steep increase of M at low fields up to a value of ca. 16 μ_B (in agreement with a $S_T = 8$ ground state), and then a slower increase, without reaching saturation at the highest field (7 T). This feature and the lack of low-temperature saturation of the $\chi_M T$ product indicate that even at the experimental lowest temperature low-lying excited states are populated. Moreover, the fact that the data is not superimposed clearly indicates the presence of magnetic anisotropy (zero field splitting, ZFS). This behavior could not be reproduced by considering that only the ground state is populated at the temperatures studied (1.83-4 K), as usually done to ascertain the value of the spin ground state and its anisotropy parameter D.[51] Hence the most probable situation is that the spin ground state of complex **4** would be $S_T = 8$, but with very low-lying excited spin-states. An $S_T = 8$ ground state would indeed be in agreement with a central Mn2–Mn5 ferromagnetic interaction, the rest of the Mn pairs being antiferromagnetically coupled. The fall of $\chi_M T$ at low temperatures is then either a consequence of intramolecular competing antiferromagnetic and ferromagnetic interactions among these pairs (note that no significant inter-molecular interactions have been observed in the crystal structure) and/or of magnetic anisotropy (ZFS).

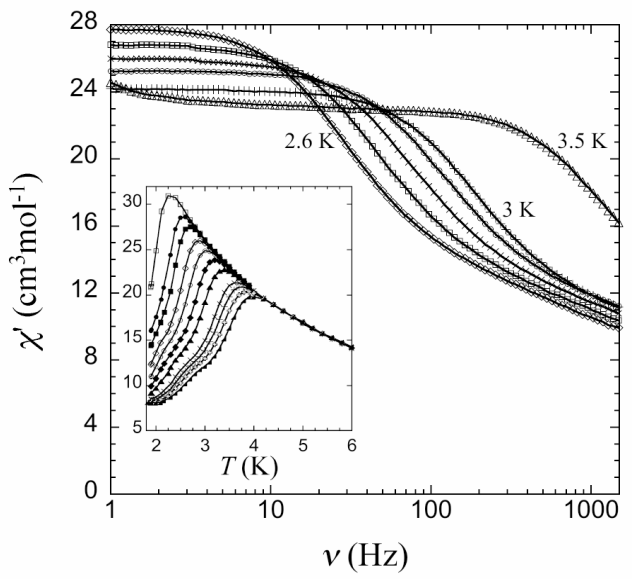

Figure 5.9: Plot of χ' *vs.* T under 0 T DC field for complex **4** (frequencies from left to right: 1, 5, 10, 25, 50, 100, 199, 498, 699, 997 and 1488 Hz). Inset: Plot of χ' *vs.* ν under 0 T DC field at temperatures between 2.6 and 3 K and 3.5 K.

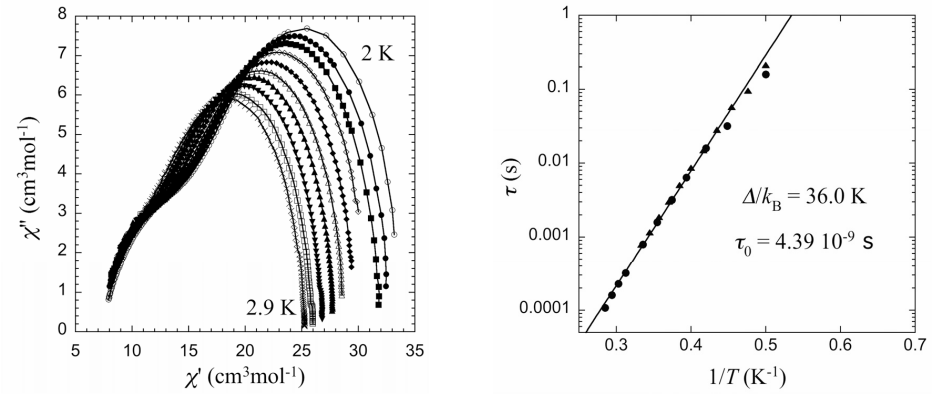

A **B**

Figure 5.10: A: Cole-Cole plots for complex **4** in the temperature range 2-2.9 K; **B:** Plot of τ *vs.* T^{-1} determined by AC measurements (full circles: temperature data, full triangles: frequency data). The solid line represents the Arrhénius fit.

Slow relaxation of the magnetization was studied using AC techniques. The frequency dependence of the AC susceptibility of a polycrystalline sample of **4** was measured at different temperatures down to 1.83 K under zero applied DC field (see Figure 5.9).

As expected for SMM, the AC susceptibilities are strongly frequency dependent indicative of a slow magnetization-relaxation phenomenon. Remarkably, blocking temperatures can be observed in **4** at reasonable temperatures, i.e. above 3 K for frequencies higher than 500 Hz (Figure 5.9). A second relaxation mode at higher frequencies, aside from the main one is observed, and confirmed by the shape of Cole-Cole plots (Figure 5.10A). This observation can be ascribed to a small impurity or to intermolecular effects.[52] From the data in Figure 5.10B, the main relaxation time τ can be determined from the maximum of χ'' as a function of both temperature and frequency. In the temperature domain studied the relaxation time follows the Arrhénius law with Δ/k_B = 36.0 K and $\tau_0 = 4.39 \times 10^{-9}$ s (for $T >$ 2.1 K), indicating that the relaxation is thermally activated. As in many SMMs, it is likely that Δ corresponds in fact to an effective barrier, resulting from the short-cut of the thermal barrier by quantum tunnelling of magnetization. In **4**, the experimental energy barrier Δ_{eff}/k_B = 36.0 K remains relatively large. The octanuclear core of **4** is thus a new addition to the still quite small number of metal ions cores in which this behavior has been observed at reasonably high temperatures.

Use of the external uncoordinated O or N atoms, and the replacement of the phenol ring by a pyridine ring would also permit the expansion of the cluster size or the creation of extended structures. In this sense, complexes **3** and **5** can be regarded as interesting building blocks for synthesizing new molecular magnets.

5.4 Concluding Remarks

Despite the fact that the simple didentate ligand HMesalim is known for over 30 years, its coordination chemistry has not been fully explored. In the present study, HMesalim has been found to give polynuclear clusters upon reaction with manganese or iron salts. Three novel, neutral manganese/iron clusters: hexanuclear, octanuclear and decanuclear, have been synthesized and structurally characterized. Although the bridging coordination mode is commonly observed for ligands containing phenoxo donors, including HEtsalim,[19, 53-55] the HMesalim ligand occupies terminal positions in these clusters.

Nevertheless, the small size of the ligand plays an important role in the aggregation of the oxo-, and methoxo-bridged clusters. Variable temperature magnetic studies show dominant antiferromagnetic interactions in the hexanuclear manganese and decanuclear iron complexes resulting in a zero-spin ground state and ferromagnetic interactions in the octanuclear manganese complex which exhibits SMM behavior. The study of the magnetic

properties of this novel cluster has revealed a rather high-energy barrier allowing the observation of thermally activated relaxation above 3 K. These observations point out the need for further thorough exploration of coordination chemistry of the ligand HMesalim, which represents an interesting new entry in the small list of chelating ligands used so far in the field of nanomagnets. The determination of the magnetic exchange interactions in these complexes has, however, not been possible due to their complex nature. The results in this chapter demonstrate the potential of the HMesalim-like ligands in obtaining new topologies of metal-clusters that could be a matter of interest for further synthetic and magnetochemical studies.

5.5 References

1. Kurtz, D. M., *Chem. Rev.* 1990, 90, 585-606.
2. Lippard, S. J., *Angew. Chem.-Int. Edit. Engl.* 1988, 27, 344-361.
3. Dismukes, G. C., in *Bioinorganic catalysis*, Reedijk, J. Ed; First edition, Marcel Dekker; Inc, New York, 1993; p 317.
4. Mukhopadhyay, S.; Mandal, S. K.; Bhaduri, S.; Armstrong, W. H., *Chem. Rev.* 2004, 104, 3981-4026.
5. Murugesu, M.; Habrych, M.; Wernsdorfer, W.; Abboud, K. A.; Christou, G., *J. Am. Chem. Soc.* 2004, 126, 4766-4767.
6. Christou, G.; Gatteschi, D.; Hendrickson, D. N.; Sessoli, R., *MRS Bull.* 2000, 25, 66-71.
7. Gatteschi, D.; Sessoli, R., *J. Magn. Magn. Mater.* 2004, 272-76, 1030-1036.
8. Tasiopoulos, A. J.; Vinslava, A.; Wernsdorfer, W.; Abboud, K. A.; Christou, G., *Angew. Chem.-Int. Edit.* 2004, 43, 2117-2121.
9. Gatteschi, D.; Sessoli, R., *Angew. Chem.-Int. Edit.* 2003, 42, 268-297.
10. Ritter, S. K., *Chem. Eng. News* 2004, 82, 29-32.
11. Sessoli, R.; Tsai, H. L.; Schake, A. R.; Wang, S. Y.; Vincent, J. B.; Folting, K.; Gatteschi, D.; Christou, G.; Hendrickson, D. N., *J. Am. Chem. Soc.* 1993, 115, 1804-1816.
12. Canada-Vilalta, C.; O'Brien, T. A.; Pink, M.; Davidson, E. R.; Christou, G., *Inorg. Chem.* 2003, 42, 7819-7829.
13. Glaser, T.; Lugger, T.; Hoffmann, R. D., *Eur. J. Inorg. Chem.* 2004, 2356-2362.
14. Barra, A. L.; Brunel, L. C.; Gatteschi, D.; Pardi, L.; Sessoli, R., *Accounts Chem. Res.* 1998, 31, 460-466.
15. Jones, L. F.; Brechin, E. K.; Collison, D.; Raftery, J.; Teat, S. J., *Inorg. Chem.* 2003, 42, 6971-6973.
16. Sessoli, R.; Gatteschi, D.; Caneschi, A.; Novak, M. A., *Nature* 1993, 365, 141-143.
17. Caneschi, A.; Gatteschi, D.; Sessoli, R.; Barra, A. L.; Brunel, L. C.; Guillot, M., *J. Am. Chem. Soc.* 1991, 113, 5873-5874.
18. Godbole, M. D.; Grigiotti, E.; Zanello, P.; Mills, A. M.; Spek, A. L.; Bouwman, E., *Inorg. Chim. Acta* 2005, 358, 233-238.
19. Godbole, M. D.; Kloskowski, M.; Hage, R.; Rompel, A.; Mills, A. M.; Spek, A. L.; Bouwman, E., *Eur. J. Inorg. Chem.* 2005, 305-313.
20. Stoss, P., *Chem. Ber.* 1978, 111, 314-319.
21. Vinkler, P.; Thimm, K.; Vob, J., *Liebigs Ann. Chem.* 1976, 1976, 2083- 2093.
22. Black, D. S. C.; Wade, M. J., *Aust. J. Chem.* 1972, 25, 1797-1810.
23. Spek, A. L. *PLATON*, Utrecht University: Utrecht (The Netherlands), 2003.
24. Sheldrick, G. M. *SHELXS-97 and SHELXL-97*, University of Göttingen: Göttingen (Germany), 1997.
25. Aromi, G.; Knapp, M. J.; Claude, J. P.; Huffman, J. C.; Hendrickson, D. N.; Christou, G., *J. Am. Chem. Soc.* 1999, 121, 5489-5499.
26. Gerritsen, H. J.; Sabisky, E. S., *Phys. Rev.* 1963, 132, 1507-1512.
27. Duraismay, T.; Ramanan, A.; Vittal, J. J., *J. Mater. Chem.* 1999, 9, 763-767.
28. Biagioli, M.; Strinna-Erre, L.; Micera, G.; Panzanelli, A.; Zema, M., *Inorg. Chem. Commun.* 1999, 2, 214-217.

29. Pessoa, J. C.; Duarte, M. T.; Gillard, R. D.; Madeira, C.; Matias, P. M.; Tomaz, I., *J. Chem. Soc. Dalton Trans.* 1998, 4015-4020.
30. Taft, K. L.; Papaefthymiou, G. C.; Lippard, S. J., *Inorg. Chem.* 1994, 33, 1510-1520.
31. Sun, Z. M.; Gantzel, P. K.; Hendrickson, D. N., *Inorg. Chem.* 1996, 35, 6640-6641.
32. Cavaluzzo, M.; Chen, Q.; Zubieta, J., *J. Chem. Soc.-Chem. Commun.* 1993, 131-133.
33. Hogerheide, M. P.; Ringelberg, S. N.; Janssen, M. D.; Boersma, J.; Spek, A. L.; van Koten, G., *Inorg. Chem.* 1996, 35, 1195-1200.
34. Kunert, M.; Dinjus, E.; Nauck, M.; Sieler, J., *Chem. Ber.-Recl.* 1997, 130, 1461-1465.
35. Boyle, T. J.; Andrews, N. L.; Rodriguez, M. A.; Campana, C.; Yiu, T., *Inorg. Chem.* 2003, 42, 5357-5366.
36. Turova, N. Y.; Turevskaya, E. P.; Kessler, V. G.; Yanovsky, A. I.; Struchkov, Y. T., *J. Chem. Soc.-Chem. Commun.* 1993, 21-23.
37. Artero, V.; Proust, A.; Herson, P.; Thouvenot, R.; Gouzerh, P., *Chem. Commun.* 2000, 883-884.
38. Tsai, H. L.; Wang, S. Y.; Folting, K.; Streib, W. E.; Hendrickson, D. N.; Christou, G., *J. Am. Chem. Soc.* 1995, 117, 2503-2514.
39. Wang, S.; Tsai, H. L.; Folting, K.; Martin, J. D.; Hendrickson, D. N.; Christou, G., *J. Chem. Soc.-Chem. Commun.* 1994, 671-673.
40. Libby, E.; Folting, K.; Huffman, C. J.; Huffman, J. C.; Christou, G., *Inorg. Chem.* 1993, 32, 2549-2556.
41. Rajaraman, G.; Murugesu, M.; Sanudo, E. C.; Soler, M.; Wernsdorfer, W.; Helliwell, M.; Muryn, C.; Raftery, J.; Teat, S. J.; Christou, G.; Brechin, E. K., *J. Am. Chem. Soc.* 2004, 126, 15445-15457.
42. Xia, X. P.; Verelst, M.; Daran, J. C.; Tuchagues, J. P., *J. Chem. Soc.-Chem. Commun.* 1995, 2155-2157.
43. Abbati, G. L.; Cornia, A.; Fabretti, A. C.; Caneschi, A.; Gatteschi, D., *Inorg. Chem.* 1998, 37, 3759-3766.
44. Caneschi, A.; Cornia, A.; Fabretti, A. C.; Gatteschi, D., *Angew. Chem.-Int. Edit. Engl.* 1996, 34, 2716-2718.
45. Asirvatham, S.; Khan, M. A.; Nicholas, K. M., *Inorg. Chem.* 2000, 39, 2006-2007.
46. Caneschi, A.; Cornia, A.; Fabretti, A. C.; Gatteschi, D.; Malavasi, W., *Inorg. Chem.* 1995, 34, 4660-4668.
47. Day, V. W.; Eberspacher, T. A.; Klemperer, W. G.; Park, C. W.; Rosenberg, F. S., *J. Am. Chem. Soc.* 1991, 113, 8190-8192.
48. Aubin, S. M. J.; Dilley, N. R.; Pardi, L.; Krzystek, J.; Wemple, M. W.; Brunel, L. C.; Maple, M. B.; Christou, G.; Hendrickson, D. N., *J. Am. Chem. Soc.* 1998, 120, 4991-5004.
49. Kambe, K., *J. Phys. Soc. Jpn.* 1950, 5, 48-51.
50. Miyasaka, H.; Clerac, R.; Ishii, T.; Chang, H. C.; Kitagawa, S.; Yamashita, M., *J. Chem. Soc.-Dalton Trans.* 2002, 1528-1534.
51. Vincent, J. B.; Christmas, C.; Chang, H. R.; Li, Q. Y.; Boyd, P. D. W.; Huffman, J. C.; Hendrickson, D. N.; Christou, G., *J. Am. Chem. Soc.* 1989, 111, 2086-2097.
52. Boskovic, C.; Bircher, R.; Tregenna-Piggott, P. L. W.; Gudel, H. U.; Paulsen, C.; Wernsdorfer, W.; Barra, A. L.; Khatsko, E.; Neels, A.; Stoeckli-Evans, H., *J. Am. Chem. Soc.* 2003, 125, 14046-14058.
53. Geiss, A.; Vahrenkamp, H., *Eur. J. Inorg. Chem.* 1999, 1793-1803.
54. Shyu, H. L.; Wei, H. H.; Wang, Y., *Inorg. Chim. Acta* 1999, 290, 8-13.
55. Aono, T.; Wada, H.; Yonemura, M.; Furutachi, H.; Ohba, M.; Okawa, H., *J. Chem. Soc.-Dalton Trans.* 1997, 3029-3034.